



Seasonal evaluation of downscaled land surface temperature: A case study in a humid tropical city



Himanshu Govil^a, Subhanil Guha^{a,*}, Anindita Dey^b, Neetu Gill^c

^a Department of Applied Geology, National Institute of Technology Raipur, Raipur, Chhattisgarh, India

^b Department of Geography, Nazrul Balika Vidyalaya, Guma, West Bengal, India

^c Chhattisgarh Council of Science and Technology, Raipur, India

ARTICLE INFO

Keywords:

Atmospheric science
Environmental science
Geography
Land surface temperature (LST)
Downscaling
TsHARP
Land use/land cover (LULC)
Landsat

ABSTRACT

The present study evaluates the seasonal variation of estimated error in downscaled land surface temperatures (LST) over a heterogeneous urban land. Thermal sharpening (TsHARP) downscaling algorithm has been used with a separate combination of four selected remote sensing indices. This study assesses the capability of TsHARP technique over mixed land use/land covers (LULC) by analyzing the correlation between LST and remote sensing indices, namely, normalized difference built-up index (NDBI), normalized difference vegetation index (NDVI), normalized difference water index (NDWI), and normalized multi-band drought index (NMDI) and by determining the root mean square error (RMSE) and mean error (ME) produced by downscaled LST. Landsat 8 OLI (Operational Land Imager) and TIRS (Thermal Infrared Sensor) images have been used for pre-monsoon, monsoon, post-monsoon, and winter seasons in 2014 covering the whole Raipur City, India. The RMSE of the downscaled LST decreases from 120 to 480 m spatial resolution in all the four seasons. It is concluded that NDBI is the most effective LULC index having the least error produced in TsHARP downscaling technique, irrespective of any season. Post-monsoon season reflects the most successful result followed by monsoon season. Even in the monsoon season of high vegetation coverage, NDBI presents a lower range of downscaled error compared to NDVI. This indicates better performance of NDBI in detecting the spatial and temporal distribution of mixed urban land.

1. Introduction

Land surface temperature (LST) is an important biophysical parameter in the processes of surface energy and water balance at regional and global scales (Anderson et al., 2008; Duan et al., 2014; Li et al., 2013; Wan and Li, 1997, 2008). LST is used in a large scale to determine soil moisture content (Voogt and Oke, 2003; Jeganathan et al., 2011; Zhan et al., 2013), to analyze the effect of urban heat island (Zakšek and Oštir, 2012; Sobrino et al., 2004; Guha et al., 2017, 2018, 2019; Zhou et al., 2019a,b), to evaluate diurnal temperature variation (Weng et al., 2004; Dennison et al., 2006; Agam et al., 2007a, 2007b; Stathopoulou and Cartalis, 2009) to calculate surface longwave radiation (Yang et al., 2011; Nichol, 2009), to compute different types of evapotranspiration (Sandholt et al., 2002; Nishii et al., 1996; Pardo-Igúzquiza et al., 2011; Gualtieri and Chettri, 2000), and to estimate surface albedo and thermal inertia (Mpelasoka et al., 2001).

Current satellite imageries, such as the Landsat, Moderate Resolution

Imaging Spectroradiometer (MODIS) and Advanced Spaceborne Thermal Emission and Reflection Radiometer (ASTER), can provide LST at different spatial, spectral, radiometric, and temporal resolutions (Moran, 1990; Kustas et al., 2003; Essa et al., 2012). Due to technical limitations, these current satellite thermal sensors reflect a balance between spatial and temporal resolutions; i.e., the high spatial resolution sensors generally have a low temporal resolution, and vice versa (Weng and Fu, 2014). In order to obtain LST at high spatial and high temporal resolutions downscaling technique is considered as an effective method (Duan and Li, 2016).

Various types of downscaling techniques have been developed to get high-resolution LST from a coarse resolution thermal infrared band (Wan and Dozier, 1996; Chen et al., 2010; Pardo-Igúzquiza and Atkinson, 2006; Zhang, 2015; Yang and Yao, 2009). Extended reviews on LST downscaling methods have been assessed so far (Zhan et al., 2013; Chen et al., 2014). The most frequently used algorithm is the DisTrad algorithm (Kustas, 2003) which was modified as the TsHARP algorithm

* Corresponding author.

E-mail address: [subhanilguha@gmail.com](mailto:suhanilguha@gmail.com) (S. Guha).

(Agam et al., 2007b) and the scale invariant relationship between the normalized difference vegetation index (NDVI) and LST is the foundation of these algorithms. The performance of these different algorithms was assessed over different land use/land cover (LULC) categories, including cultivated land (Jeganathan et al., 2011) or mixed urban land (Essa et al., 2012). The main restriction of the TsHARP algorithm is that this relationship is not unique, and thus, provides an extensive range of LST for a single NDVI value. Merlin et al. (2010) further enhanced the TsHARP algorithm by considering the effect of photosynthetically and non-photosynthetically active cells of the green plants within the spatial variability of LST. Furthermore, Bindhu et al. (2013) developed a nonlinear DisTrad (NL-DisTrad) model where NDVI-LST polynomial relationship generates from the hot-edge pixels at a coarse resolution which is also valid at high-resolution pixels.

The NDVI is not so appropriate for LST downscaling procedure performed in a heterogeneous urban land (Stathopoulou and Cartalis, 2009; Nichol, 2009; Dominguez et al., 2011; Zakšek and Oštir, 2012; Essa et al., 2012). Some recent research works reflected modern image classification techniques for detail LULC classification (Cheng et al. 2018a, 2018b; Zhou et al., 2019a,b). Different LULC types, found in a complex urban land, produce a unique emission rate. Emissivity (Stathopoulou and Cartalis, 2009; Nichol, 2009) has been used as one of the most significant environmental factors for highly heterogeneous urban landscapes. Small (2006) observed a close relationship between LST and surface albedo in urban areas. Dominguez et al. (2011) developed high-resolution urban thermal sharpener algorithm for downscaling LST in an urban area by integrating NDVI and surface albedo. Impervious surface percentage (Essa et al., 2012, 2013) and pure pixel index (Yang et al., 2010) have also been applied as basic parameters in urban areas. Impervious surface provides a better result than NDVI in LST downscaling in the mixed urban land by comparing 15 different parameters (Essa et al., 2012). Essa et al. (2012) and Yuan and Bauer (2007) also established a strong linear relationship between LST and impervious surface irrespective of the seasonal influence. Contrary to that, the LST-NDVI relationship changes with the seasonal variability (Kustas et al., 2003). For a complex urban area with mixed LULC types, multiple environmental parameters must be integrated to achieve a high downscaling precision. Although various types of LST downscaling methods have been suggested, they have also some limitations in the available remotely sensed data and LULC categories. Besides, selection of appropriate environmental predictors for LST downscaling in complex LULC surface is still considered as an important task.

Basically, the statistical downscaling of LST is based on the correlation between LST and other environmental factors or remote sensing based various LULC indices. Generally, most of the popular LST downscaling methods apply NDVI observed at a fine resolution (Kustas et al., 2003), but the NDVI alone cannot be able to explain all the variations in LST for a complex urban surface. Mukherjee et al. (2015) evaluated seasonal variation in downscaled LST in DisTrad, TsHARP, and local model using Landsat TM 5 data over a heterogeneous agricultural land in India. Bonafoni et al. (2016) attempted to retrieve LST using Landsat TM data for Florence city in Italy and proposed a traditional downscaling framework analyzing its performances using high-resolution LST airborne image. A combination of built-up and vegetation spectral indices was adopted for the LST downscaling methods using MODIS and Landsat TM data performed in Milan city, Italy (Bonafoni, 2016). A multiple regression-based LST downscaling technique using spectral mixture analysis over the heterogeneous urban area of Aprilia, Italy was also evaluated to examine the effectiveness of multiple environmental parameters (Bonafoni and Tosi, 2017). Another analytical research was performed in the Zhangye oasis and Beijing city to assess the scale effect in LST downscaling from medium to high-resolution satellite data (Zhou et al., 2016).

In the present study, linear regression based TsHARP downscaling technique has been examined with some LULC indices along with NDVI. Basically, the TsHARP technique used fractional vegetation cover and it

was analyzed in agricultural field (Agam et al., 2007a,b). Here, the technique has been evaluated on Landsat 8 OLI and TIRS data for four different seasons (pre-monsoon, monsoon, post-monsoon, and winter) in the year of 2014. The main objectives of the research were (1) to estimate the accuracy of the downscaled LST in a heterogeneous urban landscape (Raipur City of India) of humid tropical region using TsHARP technique for separate LULC indices (normalized difference vegetation index (NDVI), normalized difference water index (NDWI), normalized difference built-up index (NDBI), and normalized multi-band drought index (NMDI)) and (2) to assess the seasonal variation of the result in 2014.

2. Materials & methods

The present study has been conducted in Raipur, a tropical city of India. Raipur is considered as a heterogeneous urban area characterized by dry tropical monsoon climate. Raipur has an average elevation of 298 m, is located between 21°11'22"N to 21°20'02"N and 81°32' 20"E to 81°41'50"E (Fig. 1). Average annual temperature varies between 34 °C (in summer), and 20 °C (in winter). The area receives 90% of annual rainfall of 130 cm during June to September. This urban area is characterized by four main LULC types, namely, vegetation, water bodies, bare land, and built-up area. A high rate of land conversion (other lands to the built-up area) has been taken place in the recent time periods.

Four separate cloud-free Landsat 8 OLI and TIRS images of 5 June 2014, 25 September 2014, 12 November 2014, and 30 December 2014 were used for the evaluation of the TsHARP downscaling technique. Green, red, near infrared, shortwave infrared 1, and shortwave infrared 2 bands of 30 m spatial resolution in OLI sensor were used in determining the LULC indices and thermal infrared band of 100 m spatial resolution in TIRS sensor was used for estimating the LST.

For the convenience of LST downscaling calculation, Landsat 8 TIRS data (100-m resolution) were resampled into 30 m by the nearest neighbor method by simple raster data aggregation to coincide with Landsat 8 OLI data (30-m resolution). These aggregated OLI and TIRS data were further resampled by aggregation into 960 m. The 960-m aggregated coarse-resolution data were used to build the relationship model, whereas the 30-m reflective data were used to downscale the LST at 30 m. The 30 m retrieved LST was used to validate the 30-m downscaled LST. Subsequently, the four indices (NDVI, NDWI, NDBI, and NMDI) with 30-m resolution were then estimated from the 30-m OLI images. The final available output is the downscaled LST of 30-m resolution. The overall accuracy of the entire downscaled LST in various LULC was compared and evaluated.

2.1. Retrieval of LST using Landsat 8 OLI and TIRS data

Retrieving LST from Landsat 8 OLI and TIRS data includes the brightness temperature calculation and the emissivity correction. The at-sensor brightness temperature assumes that the Earth's surface is a black body and includes atmospheric effects (along path absorption and emissions) (Chander et al., 2009). The conversion formula from the at-sensor spectral radiance L to the at-sensor brightness temperature T_B is shown in Eq. (1). LST is retrieved by Eq. (2):

$$T_B = \frac{K_2}{\ln((K_1/L_\lambda) + 1)} \quad (1)$$

$$LST = \frac{K_2}{1 + (\lambda\sigma T_B/(hc))\ln\epsilon} \quad (2)$$

Where, T_B is the brightness temperature in Kelvin (K), L_λ is the spectral radiance in $\text{Wm}^{-2}\text{sr}^{-1}\text{mm}^{-1}$; K_2 and K_1 are calibration constants. For Landsat 8 TIRS data, K_1 is 774.89, K_2 is 1321.08. λ is the effective wavelength (11.335 μm for band 10 in Landsat 8 OLI data), σ is Boltzmann constant ($1.38 \times 10^{-23} \text{ J/K}$), h is Plank's constant (6.626×10^{-34}

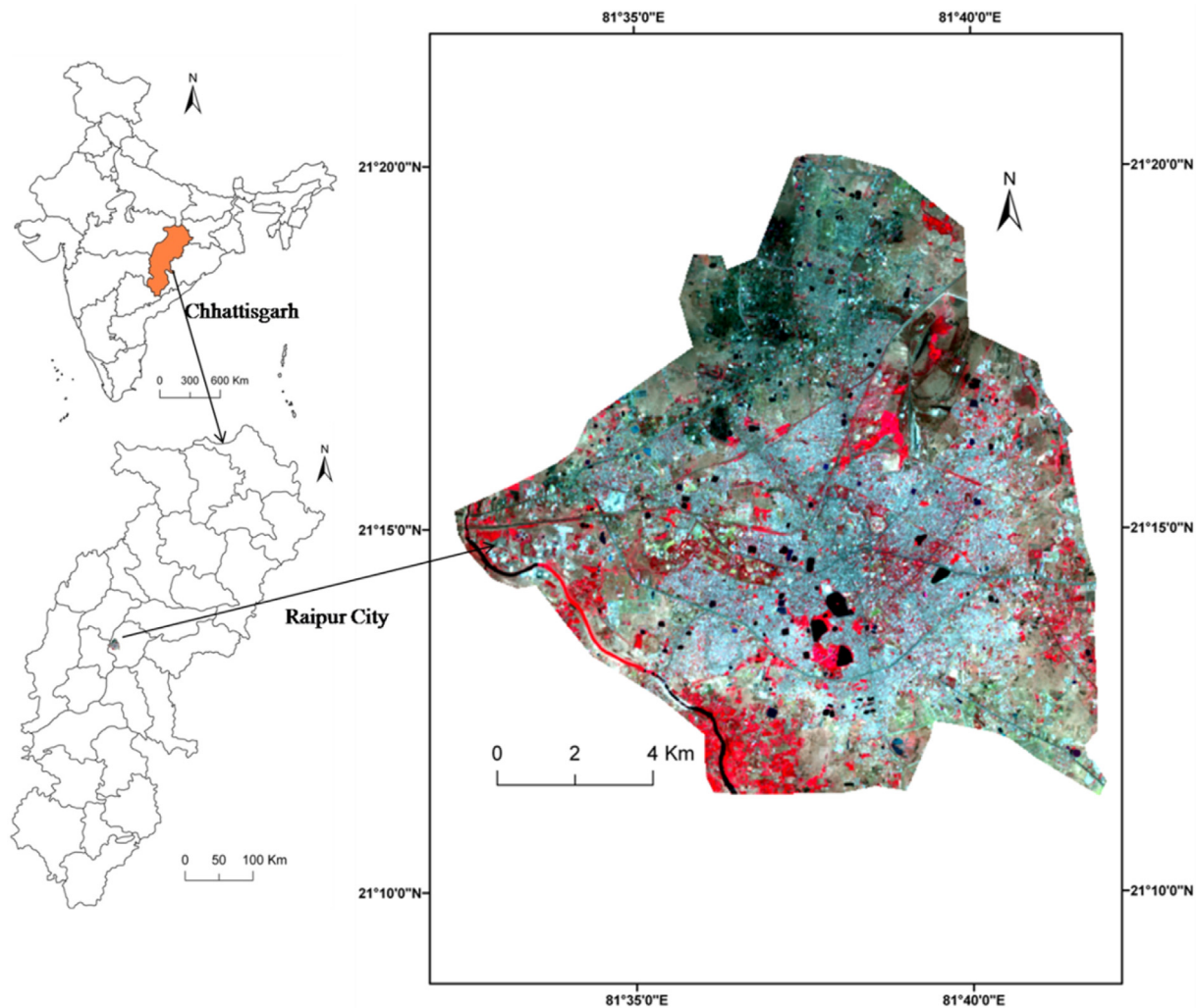


Fig. 1. Location of the study area with false colour composite image.

J , c is the velocity of light at a vacuum (2.998×10^{-8} m/s), ε is emissivity. Based on earlier studies, ε is determined as follows: if NDVI is ≥ 0.157 and ≤ 0.727 , ε for that pixel is calculated by Eq. (3) (Van et al., 1993):

$$\varepsilon = 1.0094 + 0.0047 \ln(NDVI) \quad (3)$$

The land cover type should be vegetation if NDVI values ≥ 0.727 , and then a constant value of 0.99 is assumed (Sobrino et al., 2004) and ε is set to 0.995 for water bodies and 0.92 for the other land use and land cover types.

2.2. Determination of NDVI, NDWI, NDBI, and NMDI as LULC indices

NDVI (Purevdorj et al., 1998) is considered as one of the most frequently used vegetation indices in remote sensing study. It is also applied in deriving LST and normally shows a negative regression with LST. NDWI (Gao, 1996) is generally used for water body extraction. NDBI (Zha et al., 2003) is another spectral index which was applied in this study for built-up area extraction. NMDI (Yuan and Bauer, 2007) was also used to extract the dry soil or bare land. The formulation of these four indices was presented by Table 1.

Table 1
LULC indices used for LST downscaling.

Acronym	Description	Formulation	Reference
NDVI	Normalized difference vegetation index	$\frac{NIR - Red}{NIR + Red}$	Purevdorj et al.,(1998)
NDWI	Normalized difference water index	$\frac{Green - NIR}{Green + NIR}$	Gao (1996)
NDBI	Normalized difference built-up index	$\frac{SWIR1 - NIR}{SWIR2 + NIR}$	Zha et al., (2003)
NMDI	Normalized multi-band difference index	$\frac{[NIR - (SWIR1 + SWIR2)]}{[NIR - (SWIR1 + SWIR2)]}$	Yuan and Bauer (2007)

2.3. TsHARP downscaling technique based on the regression of LST and LULC indices

LST can be derived using thermal infrared images with coarse spatial resolutions. Regression models between ancillary environmental predictors and LST have been widely established to enhance LST resolution. If the relationships between LST and the predictors do not change with the variation in the spatial resolution, a detailed LST with a high

resolution can be calculated by the predictors using such relationships. Table 1 shows the used LULC indices in the present study for estimating downscaled LST using TsHARP technique.

The original TsHARP algorithm is primarily based on the regression model of LST and fractional vegetation cover. This technique was proposed by Agam et al. (2007a,b). Basically, it was a modification of the DisTrad algorithm (Kustas et al., 2003) and was evaluated on agricultural land of Central Iowa, USA. Jeganathan et al. (2011) showed that NDVI should be used as a covariate in TsHARP technique. The present study uses NDVI, NDWI, NDBI, and NMDI as the covariates with the LST. The TsHARP algorithm was outlined in Eq. (4a–4d) where a_0 is the intercept and a_1 is the slope of the regression equations. The Eq. 4a was followed by Eq. (4b–4d) by replacing the NDVI with NDWI, NDBI, and NMDI, respectively. The fine-resolution (30 m) LST, (LST_{fine}) could be determined by the Eq. (4a–4d):

$$LST_{fine} = a_0 + a_1.NDVI_{fine} \quad (4a)$$

$$LST_{fine} = a_0 + a_1.NDWI_{fine} \quad (4b)$$

$$LST_{fine} = a_0 + a_1.NDBI_{fine} \quad (4c)$$

$$LST_{fine} = a_0 + a_1.NMDI_{fine} \quad (4d)$$

Therefore, the coarse-resolution LST (LST_{coarse}) can be determined by the Eq. (5a–5d):

$$LST_{coarse} = a_0 + a_1.NDVI_{coarse} + \Delta T_{coarse} \quad (5a)$$

$$LST_{coarse} = a_0 + a_1.NDWI_{coarse} + \Delta T_{coarse} \quad (5b)$$

$$LST_{coarse} = a_0 + a_1.NDBI_{coarse} + \Delta T_{coarse} \quad (5c)$$

$$LST_{coarse} = a_0 + a_1.NMDI_{coarse} + \Delta T_{coarse} \quad (5d)$$

Then, a residual of LST (ΔT_{coarse}) was computed as the difference between the retrieved LST (LST_{coarse}) and the corresponding observed LST (LST_{ref}) by Eq. (6) (Kustas et al., 2003):

$$\Delta T_{coarse} = LST_{ref} - LST_{coarse} \quad (6)$$

The residual ΔT_{coarse} was introduced in the algorithm to take into account part of LST spatial variability that depends on the environmental factors other than the applied predictors, such as soil moisture, emissivity or other LULC indices. The a_0 , a_1 and residual are different when different indices are used. Finally, downscaled fine-resolution (30 m) LST (LST_{down}) was estimated by the Eq. (7a–7d):

$$LST_{down} = a_0 + a_1.NDVI_{fine} + \Delta T_{coarse} \quad (7a)$$

$$LST_{down} = a_0 + a_1.NDWI_{fine} + \Delta T_{coarse} \quad (7b)$$

$$LST_{down} = a_0 + a_1.NDBI_{fine} + \Delta T_{coarse} \quad (7c)$$

$$LST_{down} = a_0 + a_1.NMDI_{fine} + \Delta T_{coarse} \quad (7d)$$

Where, the coarse-resolution regression coefficients were applied to fine-spatial resolution spectral indices, adding the residual error of the corresponding coarse-resolution image to increase the accuracy.

The NDVI-LST relationship always tends to be varied over the mixed urban landscape. In order to overcome the problem, some remote sensing indices may be tested along with NDVI to obtain higher accuracy in the downscaled LST. The multiple least-squares linear regression downscaling method with a number of predictors was applied in some recent studies (Bonafoni, 2016; Bonafoni et al., 2016). A number of remote sensing indices have also been tested individually to obtain a better downscaled LST (Essa et al., 2012). In the present study, NDVI, NDWI,

NDBI, and NMDI have been examined separately in four different dates for the downscaling method. Finally, the overall procedure of downscaling has been applied at 30 m, 120 m, 240 m, and 480 m spatial resolutions.

2.4. Accuracy assessment and validation

The LST of 100-m resolution is aggregated to 960, 480, 240, and 120-m resolution and these new aggregated data are known as reference data (LST_{ref}). The aggregated 960-m resolution LST was downscaled (LST_{down}) to 480, 240, 120, and 30-m resolution. Root mean square error (RMSE) and mean error (ME) statistics were applied to estimate the error in downscaled LST with respect to the reference LST. RMSE and ME have been calculated by the following Eq. (8) and Eq. (9), respectively.

$$RMSE = \sqrt{\left[n^{-1} \sum_{i=1}^n (LST_{down} - LST_{ref})^2 \right]} \quad (8)$$

$$ME = \sum_{i=1}^n (LST_{down} - LST_{ref}) \quad (9)$$

A complete flowchart of the entire study has been shown in Fig. 2. The computation cost of the proposed method was small as it required less time and storage space for the entire computation process.

3. Results & discussion

Fig. 3 represented the spatial distribution of reference LST at 30 m resolution and Table 2 showed the statistical information of LST at 30-m resolution in four multi-date images. Seasonal variation in the LST distribution shows a specific thermal pattern. The mean LST values in pre-monsoon, monsoon, post-monsoon, and winter season are 33.59 °C, 29.56 °C, 23.40 °C, and 22.26 °C respectively. The range of temperature is found as 13.50 °C in pre-monsoon, 12.28 °C in monsoon, 8.83 °C in post-monsoon, and 10.12 °C in the winter season, respectively. Basically, this type of heterogeneity in LST was observed due to the changes in vegetation abundance and soil moisture content. Monsoon and post-monsoon seasons are characterized by healthy vegetation and wet soil. Winter remains comparatively dry and having least standard deviation value in LST (Table 2).

Figs. 4, 5, 6, and 7 and Table 3 presents the downscaled LST using various LULC indices based TsHARP algorithm along with the retrieved reference LST in four different seasons (pre-monsoon, monsoon, post-monsoon, and winter). It is observed that the first panel (LST reference) has a smoothed pattern since the 30-m LST resolution is not an actual measurement but a resampling, and that the downscaling improve the detail at this spatial scale. It is clearly revealed that NDBI and NMDI based TsHARP algorithm generates almost similar nature in the downscaled LST while NDVI and NDWI based TsHARP algorithm has almost identical spatial distribution of downscaled LST. This particular type of spatial pattern is reflected in each and every season. The spatial pattern of downscaled LST generates from NDBI and NMDI based TsHARP technique has a similarity with retrieved reference LST where the study area achieves a higher temperature. Monsoon season indicates most identical scenario when reference LST compares with the downscaled LST, irrespective of any LULC indices based TsHARP technique.

Table 4 presents the seasonal variation of the estimated errors (RMSE and ME) produced in downscaled LST by various types of LULC indices based TsHARP algorithm. Downscaled LST at lower spatial resolution generates a greater error than downscaled LST at higher spatial resolution. It is a common phenomenon observed in each and every season and it remains constant for any LULC indices based TsHARP downscaling technique. NDBI-based TsHARP algorithm showed the best result among all the LULC indices-based TsHARP algorithm for all the season and at every resolution level as the values of RMSE of downscaled LST lie

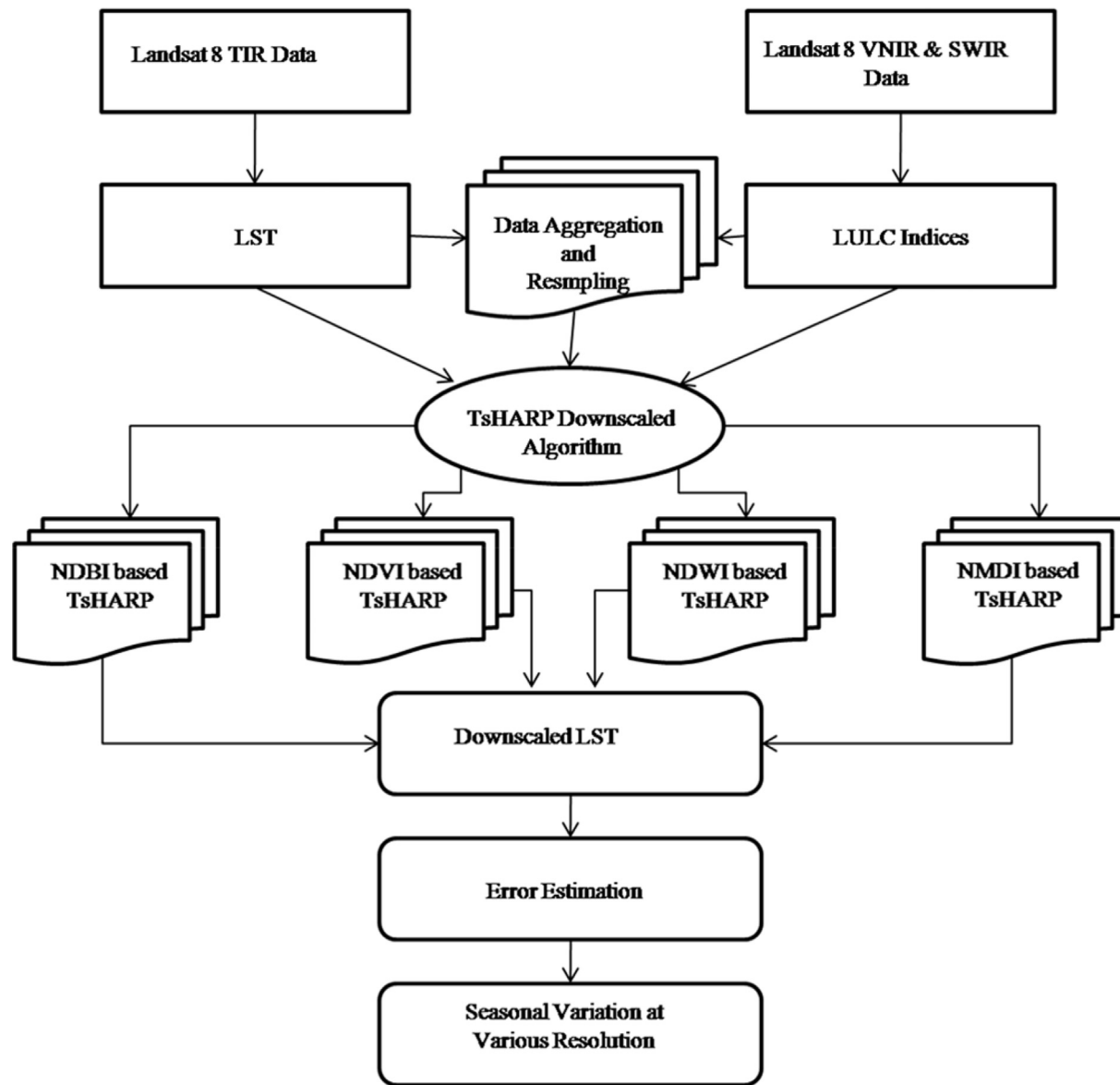


Fig. 2. Flowchart of methodology.

significantly below the standard deviation for the corresponding actual native LST reference images at 100 m spatial resolution in each and every occasion. NDBI proves as the most successful parameter for LST downscaling in almost every season. Since it is an urban area having so many mixed landscapes built-up area has the most dominant land use in controlling LST. Previously, NDVI-LST relationship based TsHARP algorithm proved as one of the most effective downscaling methods for single LULC dominated region (Agam et al., 2007a,b; Jeganathan et al., 2011). In the present study, NDVI also proves as an important indicator in determining the downscaled LST values in a heterogeneous urban landscape. Along with NDBI and NDVI, two more remote sensing indices (NDWI and NMDI) were also examined to compare the accuracy level in downscaled LST. Post-monsoon and winter season shows a better accuracy in terms RMSE and ME for any of the indices based downscaled LST. NDBI and NDMI reflect a smaller ME for pre-monsoon and winter seasons while NDVI and NDWI indicates a smaller ME in monsoon and post-monsoon seasons as an indicator used to develop TsHARP downscaling technique. Figs. 8, 9, 10, and 11 and Figs. 12, 13, 14, and 15 show the spatial distribution of RMSE and ME, respectively.

The high values of RMSE (positive) and ME (positive or negative) have mostly been found in the areas where LST is very high or

abnormally low. Due to the presence of mineral-based industrial agglomeration or thermal power plants in the northwest portions of the study area, LST generally remains high. This portion has come under one of the most erroneous zones regarding the downscaled LST. It happens mainly due to the anthropogenic activities and no such hypothetical relationship is built to support the particular behaviour.

Table 5 presents the percentage of RMSE in downscaled LST at 30 m spatial resolution for different seasons. In pre-monsoon season, NMDI and NDBI based TsHARP downscaling technique provide almost 73% of the total pixels in the study area having less than 1.5 °C RMSE in downscaled LST. NDBI again proves as the best parameter for TsHARP downscaling algorithm in monsoon season as 72.7% pixels having less than 1.5 °C RMSE. Post-monsoon season reflects the best result regarding RMSE in downscaled LST. In post-monsoon season, NDVI and NDWI based TsHARP algorithm have proved as the best output at 30 m resolution irrespective of any season as they generates downscaled LST with more than 90% pixels having less than 1.5 °C RMSE. In winter season, NDVI and NMDI based TsHARP techniques give the best result (>86% pixels have less than 1.5 °C RMSE).

Seasonal variation in the percentage of mean error (ME) in downscaled LST at 30 m resolution has been shown in Table 6. It is very clear

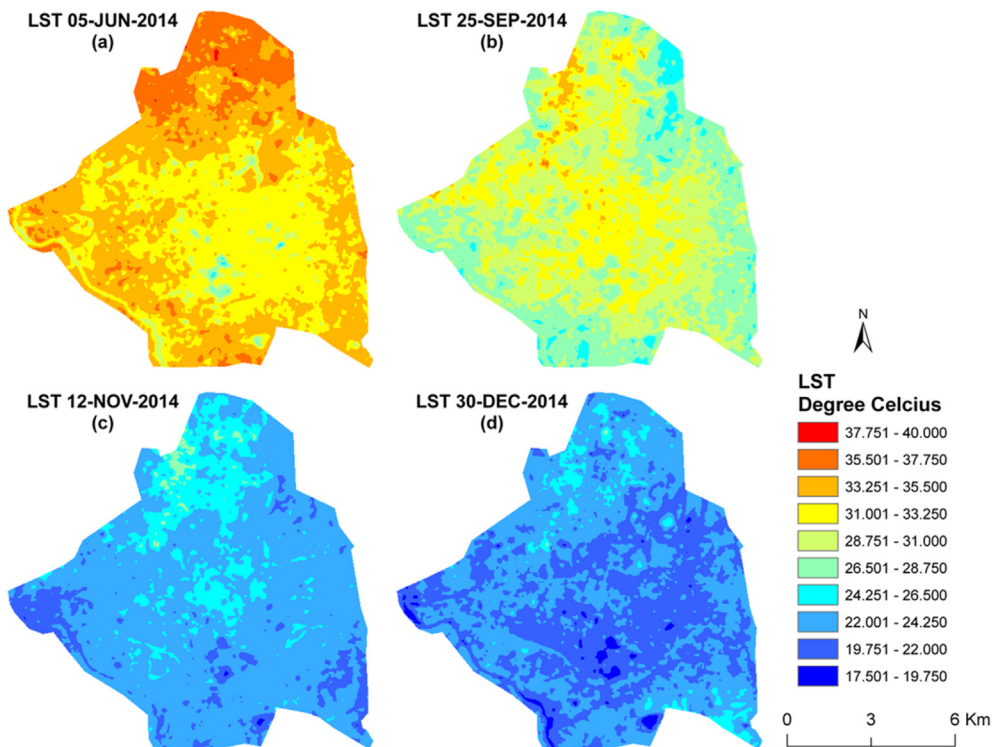


Fig. 3. Spatial distribution of reference LST at 30-m spatial resolution: (a) pre-monsoon; (b) monsoon; (c) post-monsoon; (d) winter.

Table 2
Spatial distribution of LST ($^{\circ}\text{C}$) for four multi-date reference images at 30 m resolution.

Date of Acquisition	Time	Path/Row	LST (Minimum)	LST (Maximum)	LST (Mean)	LST (Standard deviation)
05-JUN-2014	04:55:45	142/044	25.77	39.27	33.59	1.61
25-SEP-2014	04:56:11	142/044	24.51	36.79	29.56	1.73
12-NOV-2014	04:56:21	142/044	19.39	28.23	23.40	1.12
30-DEC-2014	04:56:09	142/044	17.64	27.76	22.26	1.11

from Table 6 that all the LULC indices are almost equally suitable for TsHARP downscaling technique. Post-monsoon season simply generates the best result for downscaled LST due to low pollution level, high vegetation coverage and high moisture content. NDWI and NDVI based TsHARP downscaling algorithm generates lowest level of mean error [$>75\%$ pixels have a ME from 0°C to 1°C (positive/negative)].

The study was evaluated the downscaling LST in a humid tropical city of India and reflected a good result. The similar types of studies were also performed successfully in the cities of other climatic zones, e.g., humid subtropical zone (Pan et al., 2018), temperate zone (Bechtel et al., 2012; Bonafoni et al., 2016).

The proposed work also have some limitations. The 30 m LST resolution is not an actual measurement but a resampling, and the downscaling improve the detail at this spatial scale. Only one date of a particular season may not be appropriate for seasonal assessment of downscaling technique. The other relevant LULC indices may also be incorporated to improve the downscaling results.

4. Conclusion

The aim of this research is to estimate remote sensing indices (NDBI, NDVI, NDWI, and NMDI) based downscaled LST at 30, 120, 240, and 480

m resolution and compare the results in different seasons (pre-monsoon, monsoon, post-monsoon, and winter) over a heterogeneous urban area like Raipur city. The NDVI-LST linear relationship is the primary basis of TsHARP downscaling technique. NDBI, NDWI, and NMDI are tested separately in place of NDVI to form new linear relationships, i.e., NDBI-LST, NDWI-LST, and NMDI-LST. The downscaled LST based on NDBI-LST, NDVI-LST, NDWI-LST, and NMDI-LST was finally evaluated through error estimation. The seasonal variation of the results was also determined. The results were examined at various spatial resolutions. It is clear from the various results that NDBI based TsHARP technique provides the lowest RMSE in downscaled LST at 30 m spatial resolution, irrespective of all seasons. In pre-monsoon, monsoon, and winter seasons, NDBI and NMDI based TsHARP technique have a smaller range of ME, but, in post-monsoon season, NDVI and NDWI indicate small ME due to the presence of a higher percentage of chlorophyll and moisture content. The RMSE and ME became gradually smaller with the increase of spatial resolution in downscaled LST. The LULC based TsHARP models may also be examined in determining the downscaled LST for daytime and nighttime thermal data. Different satellite sensors may also be used to assess the capability of this technique in a separate study area. Any further modification in the present TsHARP algorithm will be expected by the future researchers.

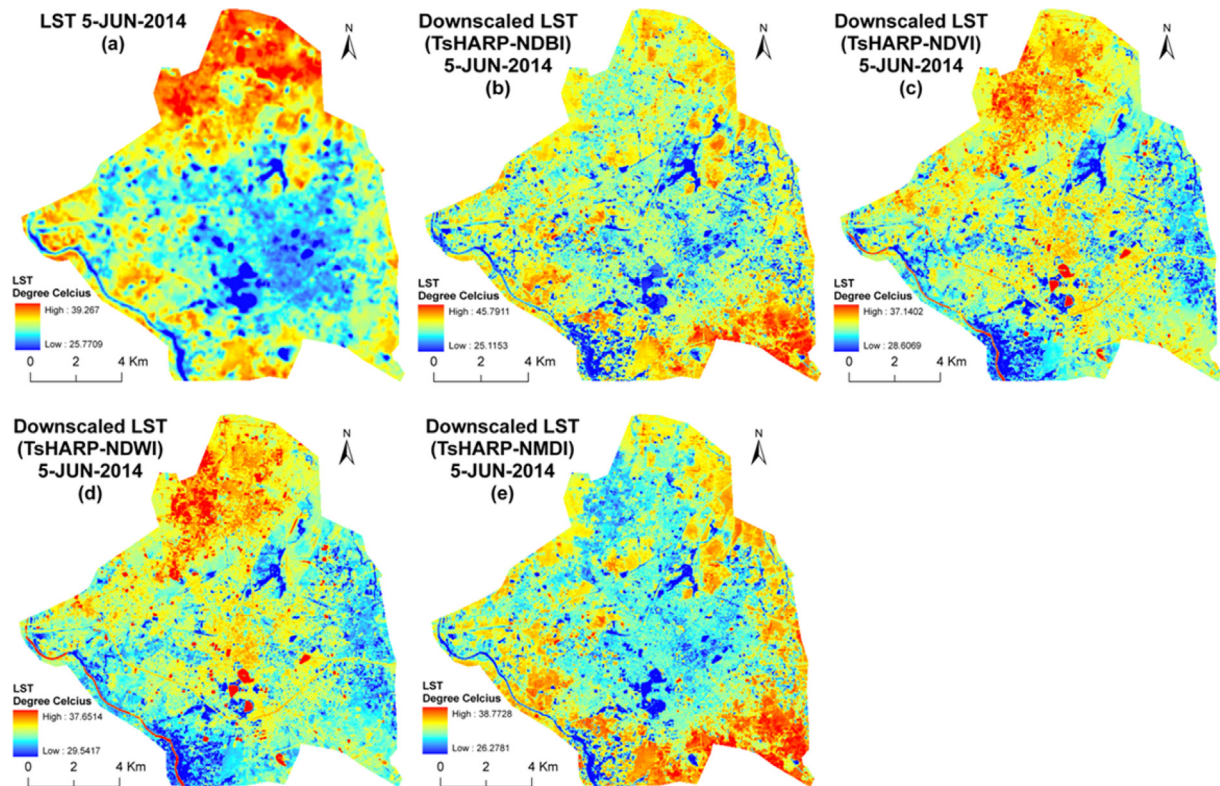


Fig. 4. Spatial distribution of retrieved LST and downscaled LST at 30-m resolution for 5-JUN-14: (a) LST_{ref} (b) NDBI-based LST_{down} ; (c) NDVI-based LST_{down} ; (d) NDWI-based LST_{down} ; (e) NMDI-based LST_{down} .

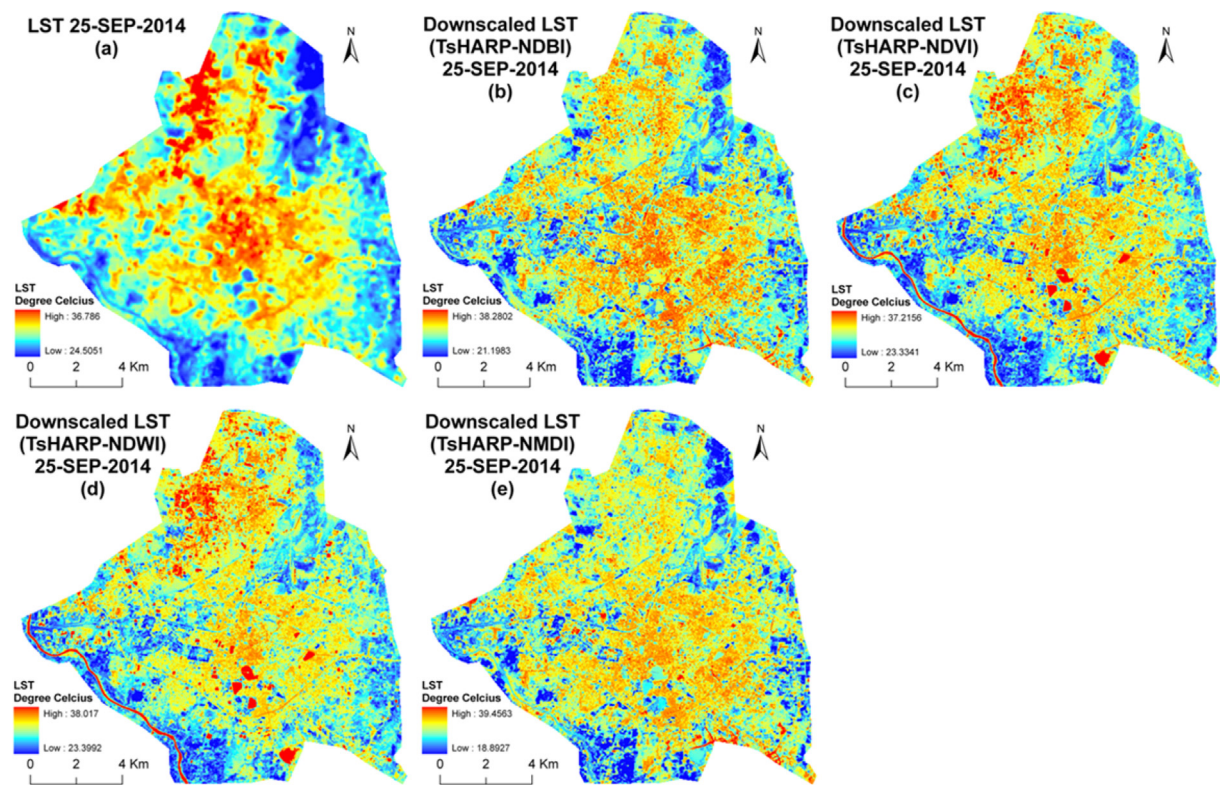


Fig. 5. Spatial distribution of retrieved LST and downscaled LST at 30-m resolution for 25-SEP-14: (a) LST_{ref} (b) NDBI-based LST_{down} ; (c) NDVI-based LST_{down} ; (d) NDWI-based LST_{down} ; (e) NMDI-based LST_{down} .

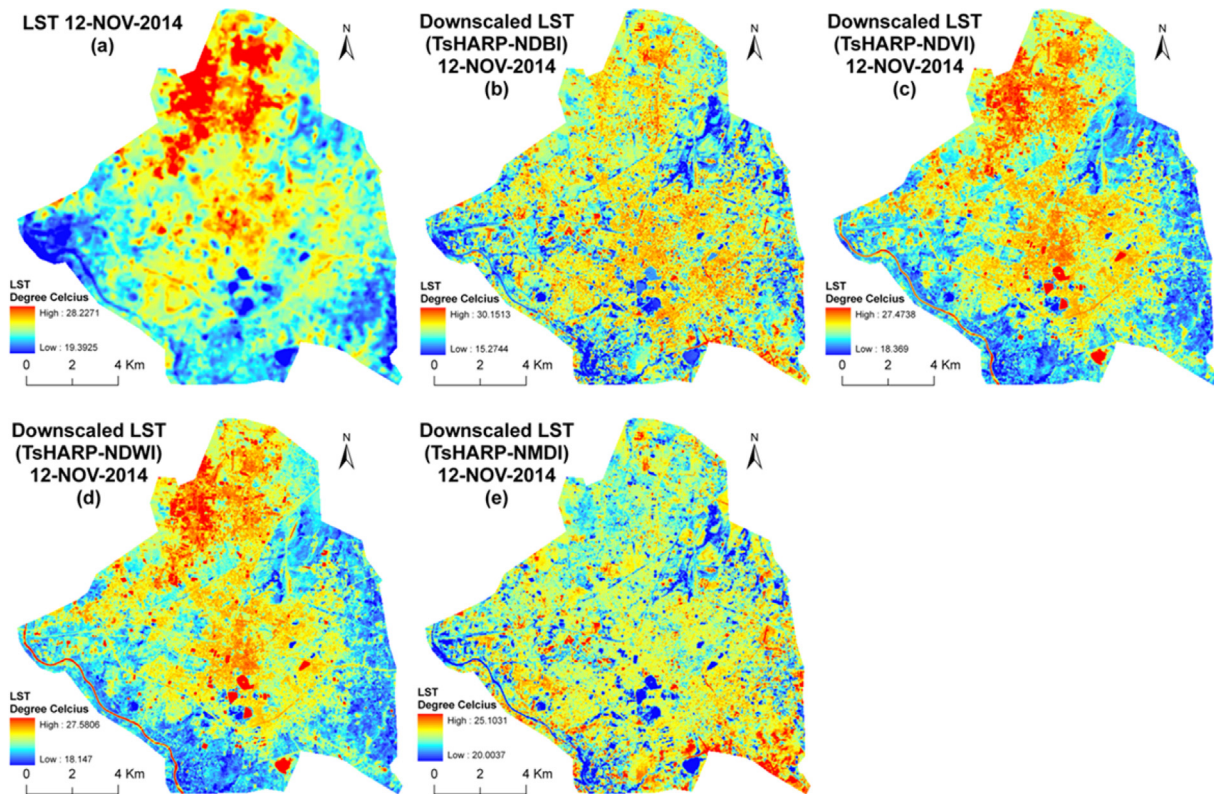


Fig. 6. Spatial distribution of retrieved LST and downscaled LST at 30-m resolution for 12-NOV-14: (a) LST_{ref} ; (b) NDBI-based LST_{down} ; (c) NDVI-based LST_{down} ; (d) NDWI-based LST_{down} ; (e) NMDI-based LST_{down} .

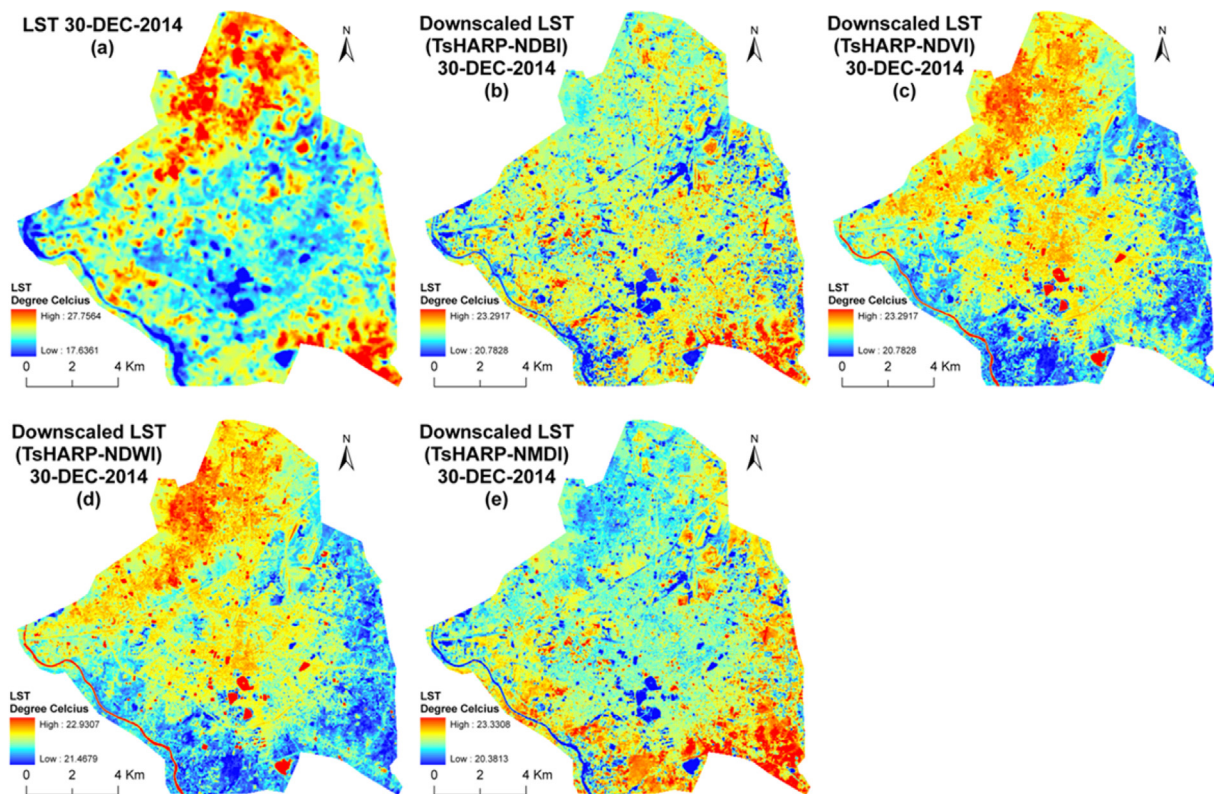


Fig. 7. Spatial distribution of retrieved LST and downscaled LST at 30-m resolution for 30-DEC-14: (a) LST_{ref} ; (b) NDBI-based LST_{down} ; (c) NDVI-based LST_{down} ; (d) NDWI-based LST_{down} ; (e) NMDI-based LST_{down} .

Table 3Seasonal variation in different LULC indices based downscaled LST ($^{\circ}\text{C}$) at various resolutions.

LULC Indices- based downscaled LST ($^{\circ}\text{C}$)	at 30 m				at 120 m				at 240 m				at 480 m			
June-05-2014																
	Min	Max	μ	σ	Min	Max	μ	σ	Min	Max	μ	σ	Min	Max	μ	σ
NDBI-based	25.77	39.27	33.59	1.61	26.33	38.14	33.62	1.58	27.01	38.06	33.64	1.52	27.98	37.09	33.69	1.42
NDVI-based	25.12	45.79	33.64	1.34	25.69	38.41	33.66	1.12	28.87	36.52	33.67	0.98	30.26	36.29	33.70	0.88
NDWI-based	28.61	37.14	33.74	0.91	29.00	36.61	33.74	0.77	30.55	35.87	33.74	0.69	31.41	35.57	33.74	0.62
NMDI-based	29.54	37.65	33.74	0.83	29.82	37.29	33.74	0.72	31.31	36.51	33.74	0.64	31.90	36.08	33.74	0.58
NDBI-based	26.28	38.77	33.64	0.93	26.28	38.78	33.64	0.93	30.96	35.98	33.67	0.72	31.39	35.64	33.69	0.66
September-25-2014																
	Min	Max	μ	σ	Min	Max	μ	σ	Min	Max	μ	σ	Min	Max	μ	σ
NDBI-based	24.51	36.79	29.56	1.73	24.59	35.89	29.54	1.71	24.67	34.76	29.52	1.65	25.26	34.49	29.46	1.57
NDVI-based	21.20	38.28	29.50	2.02	23.38	34.77	29.49	1.73	23.68	33.06	29.47	1.51	24.96	32.29	29.44	1.40
NDWI-based	23.33	37.22	29.49	2.00	24.06	35.38	29.47	1.70	24.38	34.87	29.46	1.51	25.49	33.19	29.43	1.34
NMDI-based	23.40	31.02	29.47	1.90	24.37	36.57	29.46	1.61	24.72	36.51	29.45	1.42	25.59	34.07	29.42	1.25
NDBI-based	18.89	39.46	29.47	1.87	22.38	35.56	29.45	1.58	22.75	33.44	29.44	1.41	24.54	33.22	29.42	1.26
November-12-2014																
	Min	Max	μ	σ	Min	Max	μ	σ	Min	Max	μ	σ	Min	Max	μ	σ
NDBI-based	19.39	28.23	23.40	1.12	19.53	27.92	23.39	1.11	19.66	27.37	23.38	1.07	20.26	26.96	23.36	1.02
NDVI-based	15.27	30.15	23.34	1.28	15.59	27.58	23.33	1.03	19.81	26.16	23.33	0.88	19.81	25.26	23.32	0.74
NDWI-based	18.37	27.47	23.38	1.05	19.38	26.41	23.37	0.93	20.52	26.08	23.36	0.86	21.48	25.59	23.34	0.79
NMDI-based	18.15	27.58	23.38	1.02	19.64	26.84	23.37	0.91	20.77	26.80	23.36	0.84	21.59	25.95	23.34	0.78
NDBI-based	20.00	25.10	23.30	0.28	21.31	24.39	23.31	0.22	22.45	24.07	23.31	0.19	22.48	23.97	23.31	0.15
December-30-2014																
	Min	Max	μ	σ	Min	Max	μ	σ	Min	Max	μ	σ	Min	Max	μ	σ
NDBI-based	17.63	27.76	22.26	1.11	17.68	26.86	22.27	1.08	17.78	25.79	22.28	1.03	19.08	25.41	22.29	0.94
NDVI-based	13.48	28.56	22.29	1.06	15.07	26.26	22.29	0.84	18.71	25.29	22.30	0.70	19.71	25.29	22.30	0.60
NDWI-based	20.78	23.29	22.31	0.25	21.03	23.14	22.31	0.22	21.56	23.07	22.31	0.20	21.83	22.80	22.31	0.19
NMDI-based	21.47	22.93	22.31	0.14	21.68	22.90	22.31	0.13	21.95	22.86	22.31	0.12	22.02	22.64	22.30	0.11
NDBI-based	20.38	23.33	22.29	0.17	21.30	22.93	22.29	0.14	21.79	22.79	22.29	0.13	21.89	22.75	22.30	0.11

 μ = mean, and σ = standard deviation.**Table 4**Seasonal variation in mean RMSE and mean ME for downscaled LST ($^{\circ}\text{C}$) at various resolution.

LULC indices based LST _{down}	at 30 m				at 120 m				at 240 m				at 480 m			
June-05-2014 (the standard deviation of the native LST reference image at 30 m spatial resolution is 1.61)																
	RMSE	ME	RMSE	ME	RMSE	ME	RMSE	ME	RMSE	ME	RMSE	ME	RMSE	ME	RMSE	ME
NDBI-based	1.09	0.05	0.96	0.04	0.91	0.03	0.87	0.01								
NDVI-based	1.22	0.14	1.17	0.12	1.13	0.09	1.05	0.05								
NDWI-based	1.23	0.15	1.19	0.13	1.15	0.10	1.07	0.05								
NMDI-based	1.09	0.05	1.03	0.04	0.99	0.02	0.96	0.01								
September-25-2014 (the standard deviation of the native LST reference image at 30 m spatial resolution is 1.73)																
	RMSE	ME	RMSE	ME	RMSE	ME	RMSE	ME	RMSE	ME	RMSE	ME	RMSE	ME	RMSE	ME
NDBI-based	1.11	-0.05	0.81	-0.05	0.69	-0.05	0.61	-0.03								
NDVI-based	1.21	-0.07	0.97	-0.06	0.86	-0.06	0.75	-0.04								
NDWI-based	1.25	-0.08	1.08	-0.08	0.98	-0.07	0.86	-0.04								
NMDI-based	1.18	-0.09	0.92	-0.08	0.82	-0.07	0.75	-0.05								
November-12-2014 (the standard deviation of the native LST reference image at 30 m spatial resolution is 1.12)																
	RMSE	ME	RMSE	ME	RMSE	ME	RMSE	ME	RMSE	ME	RMSE	ME	RMSE	ME	RMSE	ME
NDBI-based	0.91	-0.06	0.72	-0.05	0.65	-0.05	0.60	-0.05								
NDVI-based	0.75	-0.01	0.66	-0.02	0.60	-0.02	0.55	-0.03								
NDWI-based	0.74	-0.01	0.66	-0.02	0.60	-0.02	0.55	-0.02								
NMDI-based	0.81	-0.09	0.79	-0.08	0.78	-0.07	0.76	-0.06								
December-30-2014 (the standard deviation of the native LST reference image at 30 m spatial resolution is 1.11)																
	RMSE	ME	RMSE	ME	RMSE	ME	RMSE	ME	RMSE	ME	RMSE	ME	RMSE	ME	RMSE	ME
NDBI-based	0.85	0.03	0.71	0.03	0.65	0.02	0.59	0.01								
NDVI-based	0.86	0.05	0.84	0.05	0.79	0.04	0.73	0.01								
NDWI-based	0.86	0.05	0.84	0.04	0.80	0.03	0.72	0.01								
NMDI-based	0.81	0.03	0.79	0.03	0.76	0.02	0.69	0.01								

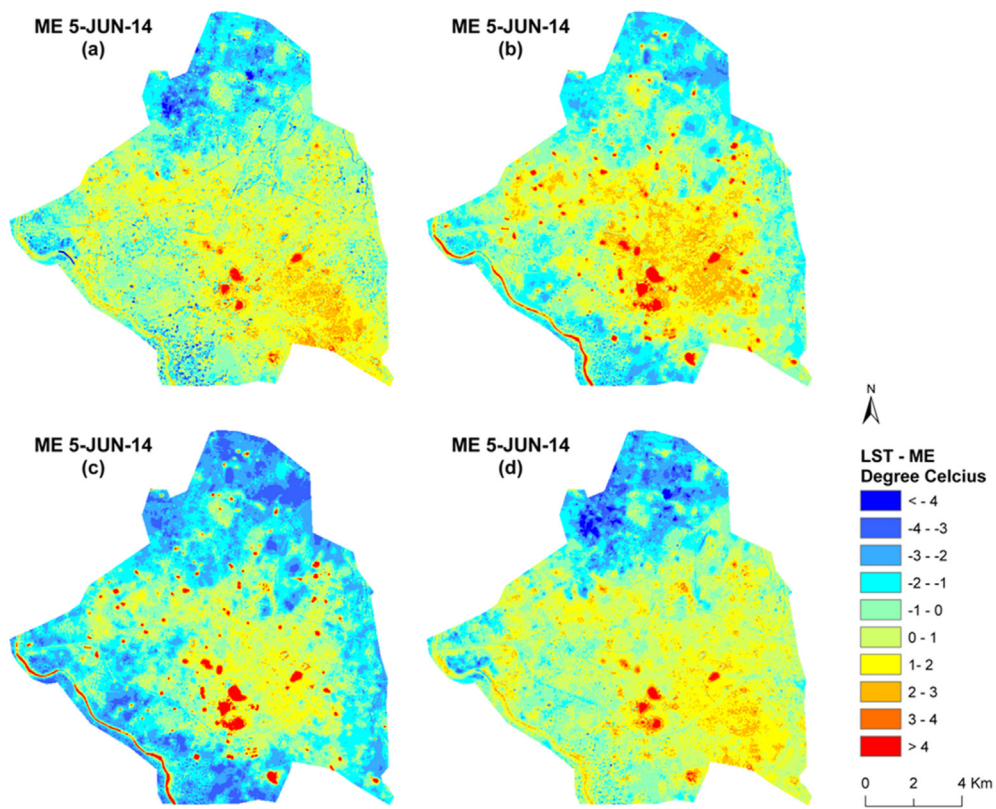


Fig. 8. Spatial distribution of ME at 30-m resolution for 5-JUN-14: (a) NDBI-based LST_{down}; (b) NDVI-based LST_{down}; (c) NDWI-based LST_{down}; (d) NMDI-based LST_{down}.

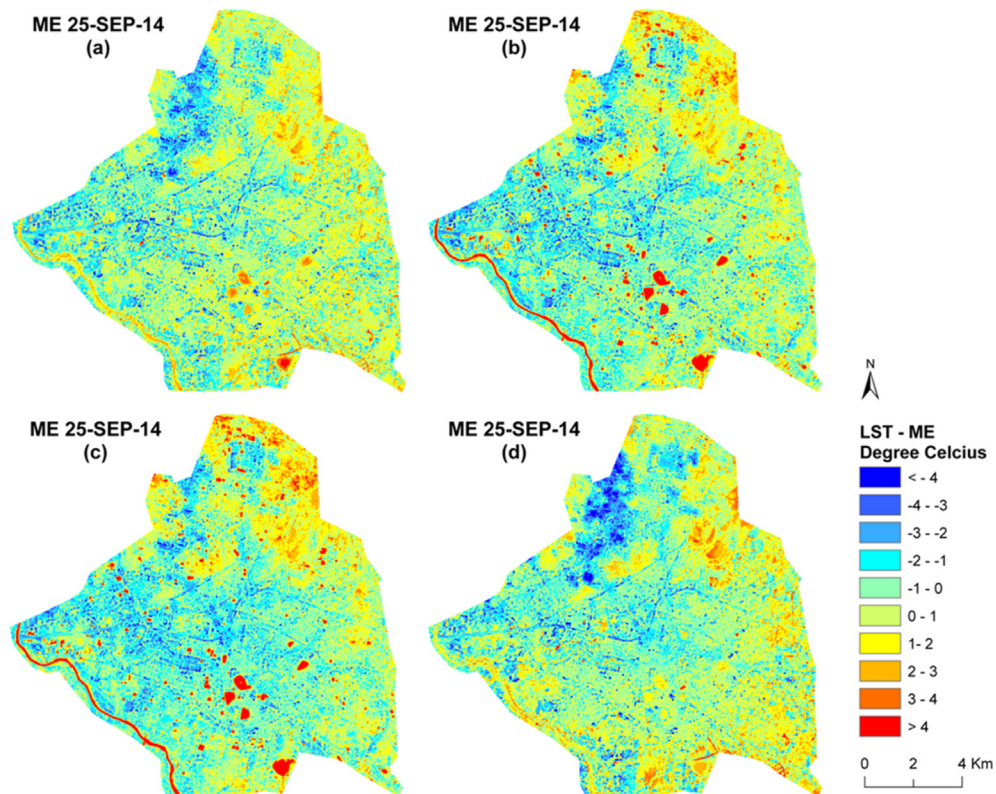


Fig. 9. Spatial distribution of ME at 30-m resolution for 25-SEP-14: (a) NDBI-based LST_{down}; (b) NDVI-based LST_{down}; (c) NDWI-based LST_{down}; (d) NMDI-based LST_{down}.

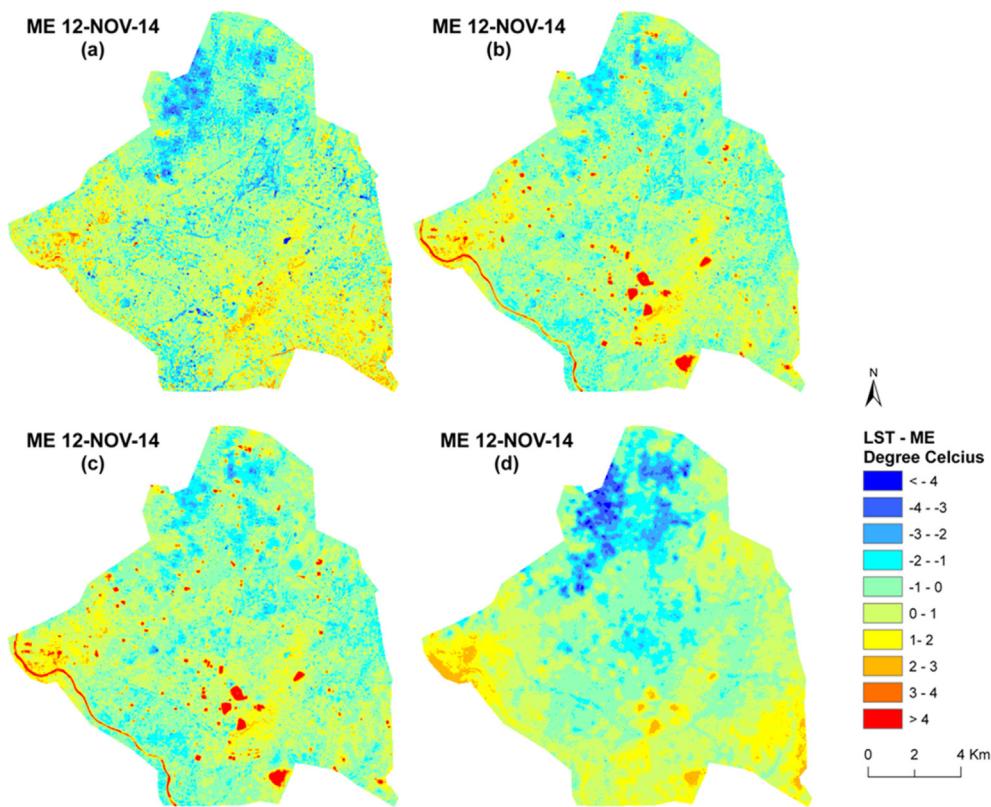


Fig. 10. Spatial distribution of ME at 30-m resolution for 12-NOV-14: (a) NDBI-based LST_{down} ; (b) NDVI-based LST_{down} ; (c) NDWI-based LST_{down} ; (d) NMDI-based LST_{down} .

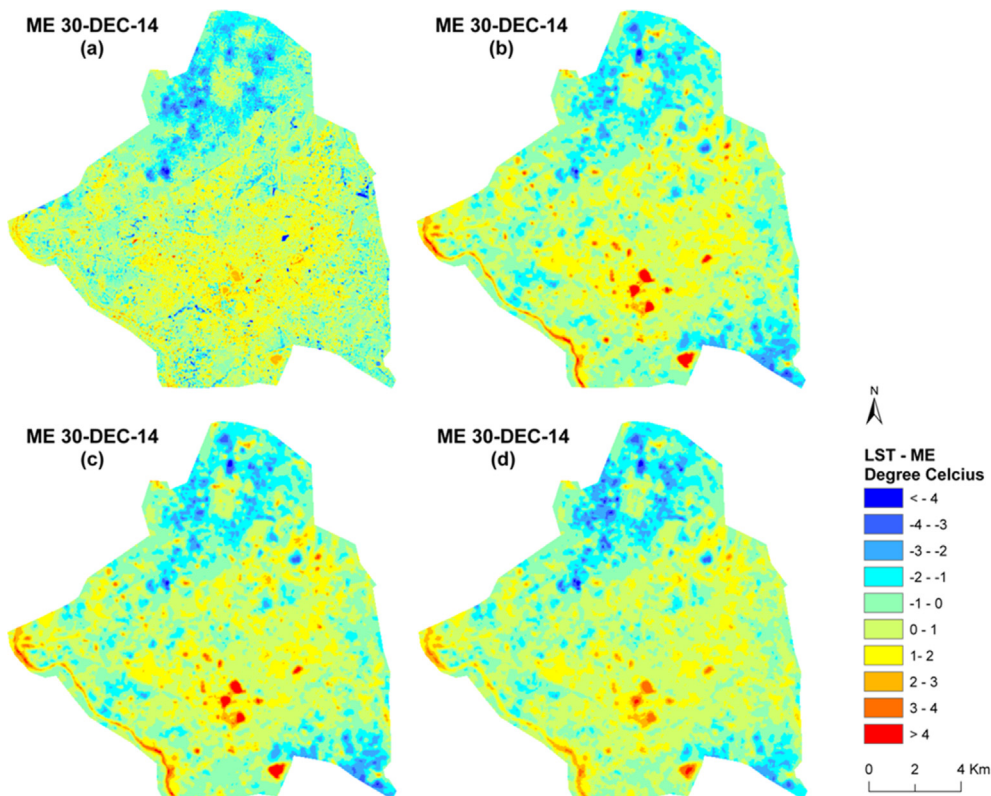


Fig. 11. Spatial distribution of ME at 30-m resolution for 30-DEC-14: (a) NDBI-based LST_{down} ; (b) NDVI-based LST_{down} ; (c) NDWI-based LST_{down} ; (d) NMDI-based LST_{down} .

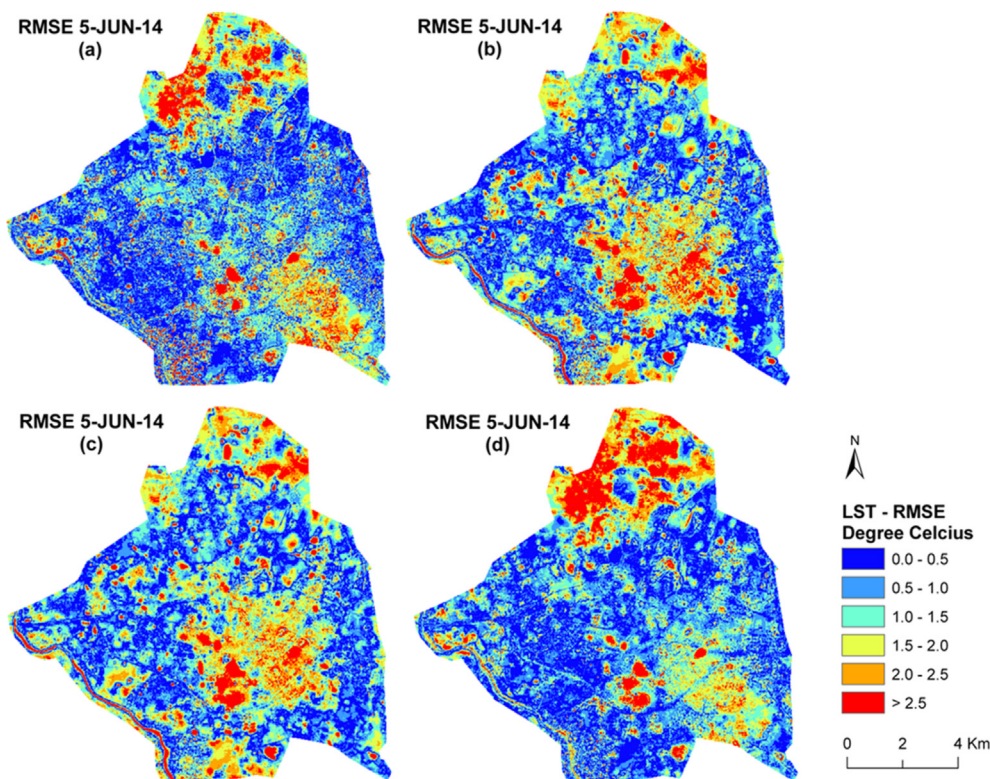


Fig. 12. Spatial distribution of RMSE at 30-m resolution for 5-JUN-14: (a) NDBI-based LST_{down}; (b) NDVI-based LST_{down}; (c) NDWI-based LST_{down}; (d) NMDI-based LST_{down}.

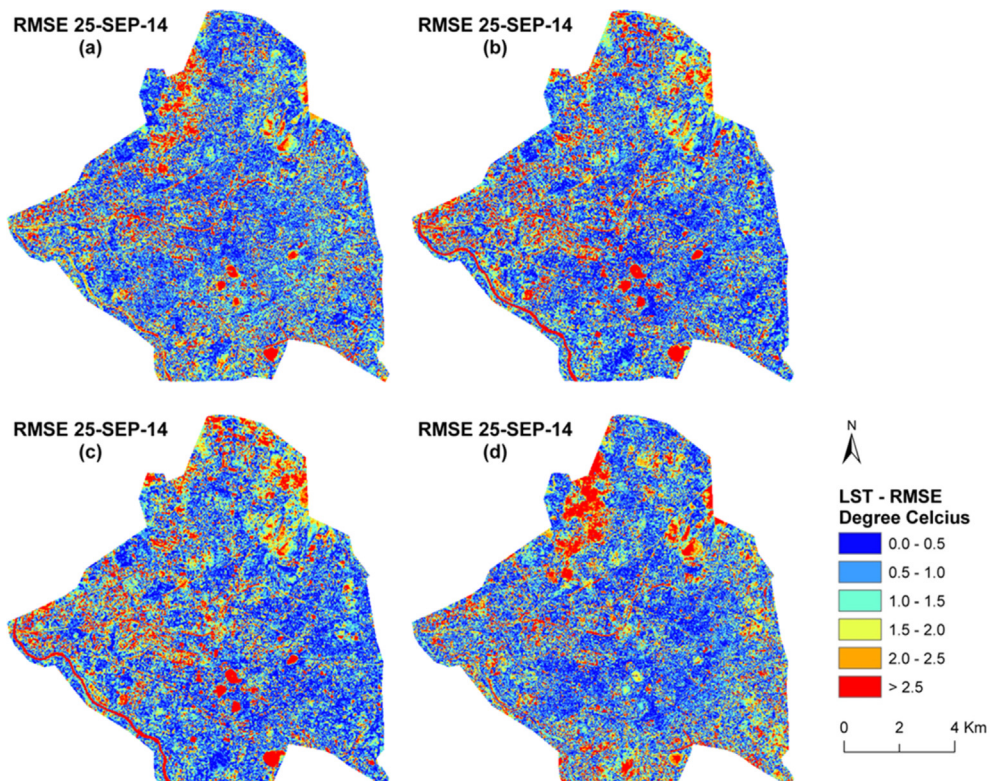


Fig. 13. Spatial distribution of RMSE at 30-m resolution for 25-SEP-14: (a) NDBI-based LST_{down}; (b) NDVI-based LST_{down}; (c) NDWI-based LST_{down}; (d) NMDI-based LST_{down}.

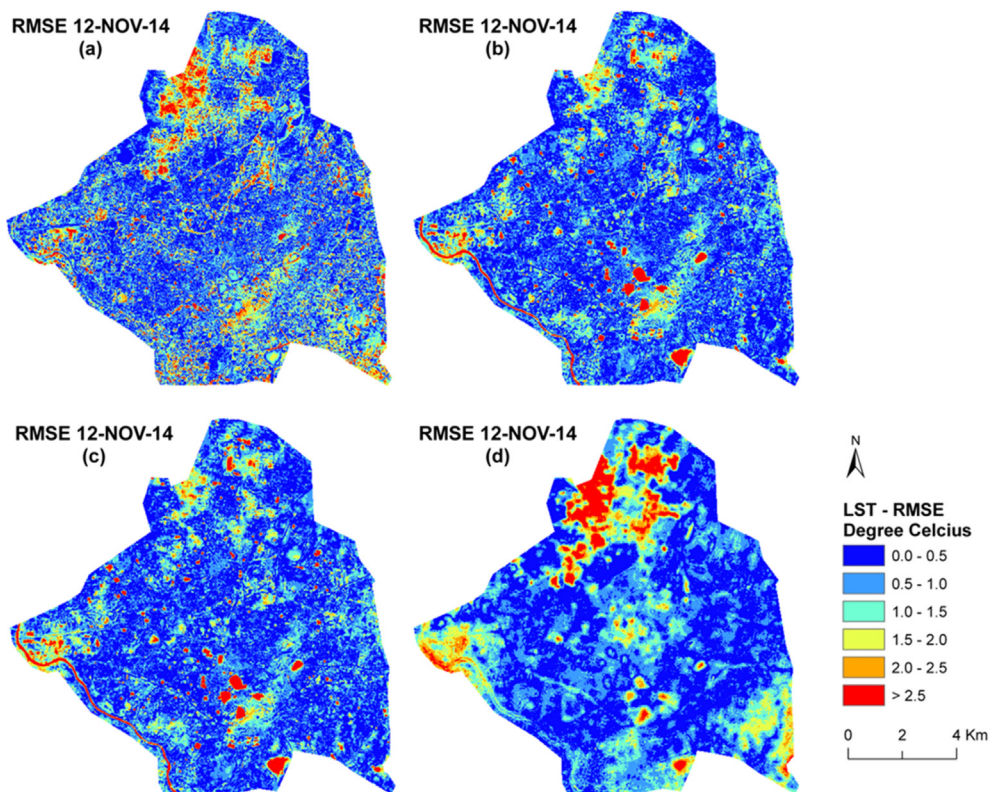


Fig. 14. Spatial distribution of RMSE at 30-m resolution for 12-NOV-14: (a) NDBI-based LST_{down} ; (b) NDVI-based LST_{down} ; (c) NDWI-based LST_{down} ; (d) NMDI-based LST_{down} .

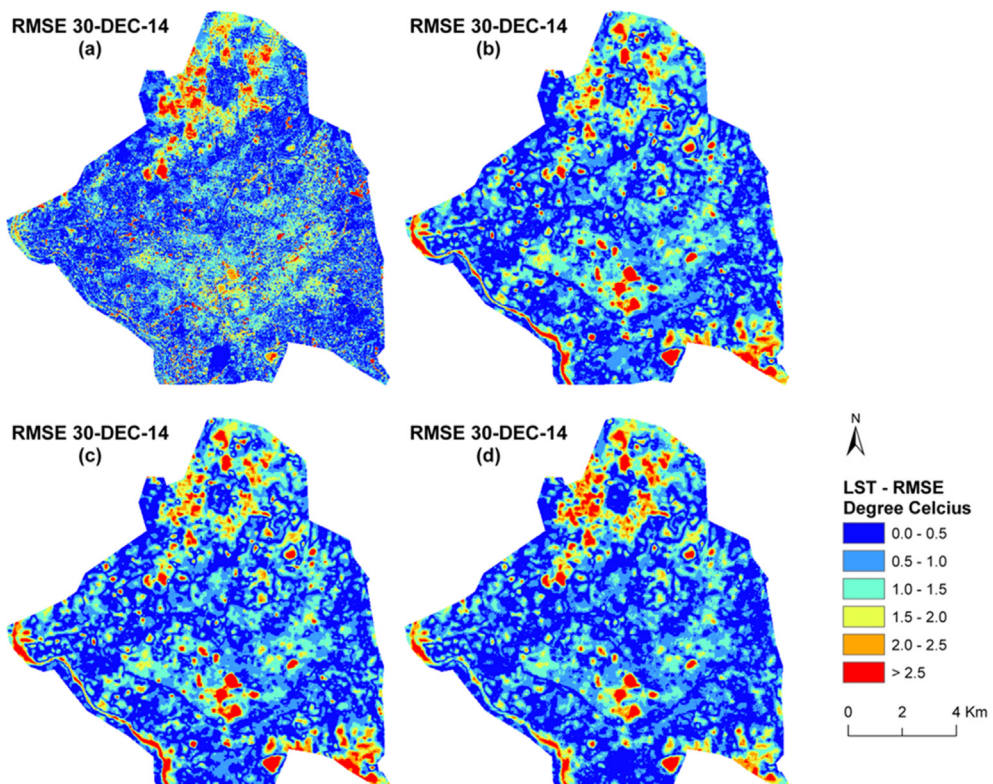


Fig. 15. Spatial distribution of RMSE at 30-m resolution for 30-DEC-14: (a) NDBI-based LST_{down} ; (b) NDVI-based LST_{down} ; (c) NDWI-based LST_{down} ; (d) NMDI-based LST_{down} .

Table 5Percentage of root mean square error (RMSE) in downscaled LST ($^{\circ}\text{C}$) at 30 m resolution.

RMSE in downscaled LST ($^{\circ}\text{C}$)	0.0–0.5	0.5–1.0	1.0–1.5	1.5–2.0	2.0–2.5	>2.5
June-05-2014						
NDBI-based	28.70%	24.43%	19.52%	13.66%	7.34%	6.35%
NDVI-based	24.00%	23.13%	19.00%	16.33%	9.43%	6.46%
NDWI-based	23.94%	23.10%	20.60%	16.46%	9.54%	6.36%
NMDI-based	29.46%	25.80%	18.61%	11.86%	6.86%	7.41%
September-25-2014						
NDBI-based	28.82%	25.27%	18.61%	11.91%	7.28%	8.13%
NDVI-based	29.49%	24.26%	17.51%	11.49%	7.03%	10.22%
NDWI-based	28.66%	24.09%	17.78%	11.87%	7.06%	10.54%
NMDI-based	28.29%	23.80%	17.92%	12.29%	7.72%	9.98%
November-12-2014						
NDBI-based	30.07%	27.52%	17.58%	9.91%	5.19%	3.74%
NDVI-based	43.58%	31.52%	14.98%	5.50%	1.81%	2.61%
NDWI-based	46.43%	30.42%	13.77%	4.91%	1.60%	2.87%
NMDI-based	41.28%	30.01%	14.26%	7.18%	3.47%	3.80%
December-30-2014						
NDBI-based	36.98%	28.71%	18.75%	9.13%	3.74%	2.70%
NDVI-based	35.47%	31.16%	19.47%	7.30%	3.29%	3.35%
NDWI-based	36.28%	30.67%	18.31%	7.54%	3.62%	3.58%
NMDI-based	39.58%	30.55%	16.15%	7.14%	3.64%	2.94%

Table 6Percentage of mean error (ME) in downscaled LST ($^{\circ}\text{C}$) at 30 m resolution.

ME in downscaled LST ($^{\circ}\text{C}$)	< -4	-4–3	-3–2	-2–1	-1–0	0–1	1–2	2–3	3–4	>4
June-05-2014										
NDBI-based	0.40%	1.61%	5.90%	13.79%	23.35%	29.78%	19.39%	4.80%	0.61%	0.36%
NDVI-based	0.01%	0.29%	5.00%	19.48%	25.89%	21.25%	17.53%	7.89%	1.06%	1.63%
NDWI-based	0.01%	0.32%	5.47%	19.18%	25.36%	21.67%	17.88%	7.18%	1.01%	1.92%
NMDI-based	0.57%	2.26%	6.93%	10.70%	21.39%	33.86%	19.77%	3.59%	0.58%	0.35%
September-25-2014										
NDBI-based	0.61%	2.15%	6.65%	14.35%	24.53%	29.56%	16.16%	4.77%	1.01%	0.20%
NDVI-based	0.62%	2.29%	6.99%	16.35%	27.62%	26.13%	12.65%	4.06%	1.09%	2.20%
NDWI-based	0.47%	2.06%	7.22%	18.24%	29.85%	22.90%	11.41%	4.00%	1.23%	2.62%
NMDI-based	1.11%	2.68%	6.79%	14.37%	25.42%	26.68%	15.84%	5.47%	1.36%	0.29%
November-12-2014										
NDBI-based	0.14%	0.85%	4.57%	13.97%	30.98%	32.6%	13.52%	2.88%	0.41%	0.06%
NDVI-based	0.01%	0.04%	1.03%	12.45%	41.24%	33.86%	8.03%	1.52%	0.78%	1.04%
NDWI-based	0.01%	0.04%	0.95%	11.73%	43.41%	33.49%	6.95%	1.33%	0.74%	1.41%
NMDI-based	0.18%	1.55%	3.80%	10.12%	34.98%	36.31%	11.32%	1.73%	0.01%	0.01%
December-30-2014										
NDBI-based	0.19%	0.80%	3.68%	11.13%	29.75%	35.93%	16.75%	1.62%	0.12%	0.03%
NDVI-based	0.03%	0.37%	3.11%	12.55%	30.79%	35.84%	14.17%	1.86%	0.74%	0.54%
NDWI-based	0.04%	0.48%	3.43%	12.30%	30.19%	36.76%	13.55%	2.02%	0.75%	0.46%
NMDI-based	0.07%	0.65%	3.62%	11.19%	28.49%	41.64%	12.10%	1.68%	0.51%	0.05%

Declarations*Additional information**Author contribution statement*

No additional information is available for this paper.

Guha, S. Govil, H. Dey, A. Gill, N.: Conceived and designed the analysis; Performed the experiments; Analyzed and interpreted the data; Contributed analysis tools or data; Wrote the paper.

Funding statement

This research did not receive any specific grant from funding agencies in the public, commercial, or not-for-profit sectors.

Competing interest statement

The authors declare no conflict of interest.

Acknowledgements

The authors thank to United States Geological Survey and National Institute of Technology Raipur, India. The authors also thank the anonymous reviewers for their relevant comments.

References

- Agam, N., Kustas, W.P., Anderson, M.C., Li, F.Q., Colaizzi, P.D., 2007a. Utility of thermal sharpening over Texas high plains irrigated agricultural fields. *J. Geophys. Res.* 112 (D19110).
- Agam, N., Kustas, W.P., Anderson, M.C., Li, F.Q., Neale, C.M.U., 2007b. A vegetation index based technique for spatial sharpening of thermal imagery. *Rem. Sens. Environ.* 107, 545–558.

- Anderson, M.C., Norman, J.M., Kustas, W.P., Houborg, R., Starks, P.J., Agam, N., 2008. A thermal-based remote sensing technique for routine mapping of land-surface carbon, water and energy fluxes from field to regional scales. *Rem. Sens. Environ.* 112 (12), 4227–4241.
- Bechtel, B., Zaksek, K., Hoshyarpour, G., 2012. Downscaling land surface temperature in an urban area: a case study for hamburg, Germany. *Rem. Sens.* 4, 3184–3200.
- Bindhu, V.M., Narasimhan, B., Sudheer, K.P., 2013. Development and verification of a nonlinear disaggregation method (NL-DisTrad) to downscale MODIS land surface temperature to the spatial scale of Landsat thermal data to estimate evapotranspiration. *Rem. Sens. Environ.* 135, 118–129.
- Bonafoni, S., Anniballe, R., Gioli, B., Toscano, P., 2016. Downscaling landsat land surface temperature over the urban area of florence. *Eur. J. Remote Sens.* 49 (1), 553–569.
- Bonafoni, S., 2016. Downscaling of Landsat and MODIS land surface temperature over the heterogeneous urban area of Milan. *IEEE J. Sel. Top. Appl. Earth Obs. Remote Sens.* 9 (5), 2019–2027.
- Bonafoni, S., Tosi, G., 2017. Downscaling of land surface temperature using airborne high-resolution data: a case study on Aprilia, Italy. *IEEE Geosci. Remote Sens. Lett.* 14 (1), 107–111.
- Chander, G., Markham, B.L., Helder, D.L., 2009. Summary of current radiometric calibration coefficients for landsat MSS, TM, ETM+, and EO-1 ALI sensors. *Rem. Sens. Environ.* 113 (5), 893–903.
- Cheng, G., Li, Z., Han, J., Yao, X., Guo, L., 2018a. Exploring hierarchical convolutional features for hyperspectral image classification. *IEEE Trans. Geosci. Remote Sens.* 56 (11), 6712–6722.
- Cheng, G., Yang, C., Yao, X., Guo, L., Han, J., 2018b. When deep learning meets metric learning: remote sensing image scene classification via learning discriminative CNNs. *IEEE Trans. Geosci. Remote Sens.* 56 (5), 2811–2821.
- Chen, L., Yan, G.J., Ren, H.Z., Li, A.H., 2010. A modified vegetation index based algorithm for thermal imagery sharpening. *IEEE Int. Geosci. Remote Sens. Symp. IGARSS* 10.
- Chen, Y., Zhan, W., Quan, J., Zhou, J., Zhu, X., Sun, H., 2014. Disaggregation of remotely sensed land surface temperature: a generalized paradigm. *IEEE Trans. Geosci. Remote Sens.* 52 (9), 5952–5965.
- Dennison, P.E., Charoensiri, K., Roberts, D.A., Peterson, S.H., Green, R.O., 2006. Wildfire temperature and land cover modeling using hyperspectral data. *Rem. Sens. Environ.* 100 (2), 212–222.
- Dominguez, A., Kleissl, J., Luval, J.C., Rickman, D.L., 2011. High-resolution urban thermal sharpener (HUTS). *Rem. Sens. Environ.* 115 (7), 1772–1780.
- Duan, S.B., Li, Z.L., 2016. Spatial downscaling of MODIS land surface temperatures using geographically weighted regression: case study in northern China. *IEEE Trans. Geosci. Remote Sens.* 54 (11), 6458–6469.
- Duan, S.B., Li, Z.L., Tang, B.H., Wu, H., Tang, R., 2014. Generation of a time-consistent land surface temperature product from MODIS data. *Rem. Sens. Environ.* 150, 339–349.
- Essa, W., van der Kwast, J., Verbeiren, B., Batelaan, O., 2013. Downscaling of thermal images over urban areas using the land surface temperature–impervious percentage relationship. *Int. J. Appl. Earth Obs. Geoinf.* 23, 95–108.
- Essa, W., Verbeiren, B., van der Kwast, J., van de Voorde, T., Batelaan, O., 2012. Evaluation of the DisTrad thermal sharpening methodology for urban areas. *Int. J. Appl. Earth Obs. Geoinf.* 19, 163–172.
- Gao, B.C., 1996. NDWI: a normalized difference water index for remote sensing of vegetation liquid water from space. *Rem. Sens. Environ.* 58, 257–266.
- Gualtieri, J.A., Chettri, S., 2000. Support Vector Machines for classification of hyperspectral data. In: Proceedings of the 2000 International Geoscience and Remote Sensing Symposium (IGARSS 2000), Honolulu, HI, USA, 24–28 July 2000. IEEE, Honolulu, HI, USA, pp. 813–815, 2000.
- Guha, S., Govil, H., Dey, A., Gill, N., 2018. Analytical study of land surface temperature with NDVI and NDBI using Landsat 8 OLI and TIRS data in Florence and Naples city, Italy. *Eur. J. Remote Sens.* 51 (1), 667–678.
- Guha, S., Govil, H., Diwan, P., 2019. Analytical study of seasonal variability in land surface temperature with normalized difference vegetation index, normalized difference water index, normalized difference built-up index, and normalized multiband drought index. *J. Appl. Remote Sens.* 13 (2), 024518.
- Guha, S., Govil, H., Mukherjee, S., 2017. Dynamic analysis and ecological evaluation of urban heat islands in Raipur City, India. *J. Appl. Remote Sens.* 11 (3), 036020.
- Jeganathan, C., Hamm, N.A.S., Mukherjee, S., Atkinson, P.M., Raju, P.L.N., Dadhwal, V.K., 2011. Evaluating a thermal image sharpening model over a mixed agricultural landscape in India. *Int. J. Appl. Earth Obs. Geoinf.* 13 (2), 178–191.
- Kustas, W.P., Norman, J.M., Anderson, M.C., French, A.N., 2003. Estimating subpixel surface temperatures and energy fluxes from the vegetation index–radiometric temperature relationship. *Rem. Sens. Environ.* 85 (4), 429–440.
- Li, Z.L., Tang, B.H., Wu, Hua., Ren, H., Yan, G., Wan, Z., Trigo, I.F., Sobrino, J.A., 2013. Satellite-derived land surface temperature: current status and perspectives. *Rem. Sens. Environ.* 131, 14–37.
- Merlin, O., Duchemin, B., Hagolle, O., Jacob, F., Coudert, B., Chehbouni, G., Dedieu, G., Garatza, J., Kerr, Y., 2010. Disaggregation of MODIS surface temperature over an agricultural area using a time series of Formosat-2 images. *Rem. Sens. Environ.* 114 (11), 2500–2512.
- Moran, M.S., 1990. A window-based technique for combining Landsat Thematic Mapper thermal data with higher-resolution multispectral data over agricultural lands. *Photogramm. Eng. Rem. Sens.* 56 (3), 337–342.
- Mpelasoka, F.S., Mullan, A.B., Heerdegen, R.G., 2001. New Zealand climate change information derived by multivariate statistical and artificial neural networks approaches. *Int. J. Climatol.* 21, 1415–1433.
- Mukherjee, S., Joshi, P.K., Garg, R.D., 2015. Evaluation of LST downscaling algorithms on seasonal thermal data in humid subtropical regions of India. *Int. J. Remote Sens.* 36 (10), 2503–2523.
- Nichol, J., 2009. An emissivity modulation method for spatial enhancement of thermal satellite images in urban heat island analysis. *Photogramm. Eng. Rem. Sens.* 75 (5), 547–556.
- Nishii, R., Kusanobu, S., Tanaka, S., 1996. Enhancement of low spatial resolution image based on high resolution bands. *IEEE Trans. Geosci. Remote Sens.* 34 (5), 1151–1158.
- Pan, X., Zhu, X., Yang, Y., Cao, C., Zhang, X., Shan, L., 2018. Applicability of downscaling land surface temperature by using normalized difference sand index. *Sci. Rep.* 8, 9530.
- Pardo-Igúzquiza, E., Chica-Olmo, M., Atkinson, P.M., 2006. Downscaling cokriging for image sharpening. *Rem. Sens. Environ.* 102, 86–98.
- Pardo-Igúzquiza, E., Rodríguez-Galiano, V.F., Chica-Olmo, M., Atkinson, P.M., 2011. Image fusion by spatially adaptive filtering using downscaling cokriging. *ISPRS J. Photogrammetry Remote Sens.* 66 (3), 337–346.
- Purevdorj, T.S., Tateishi, R., Ishiyama, T., Honda, Y., 1998. Relationships between percent vegetation cover and vegetation indices. *Int. J. Remote Sens.* 19, 3519–3535.
- Sandholt, I., Rasmussen, K., Andersen, J., 2002. A simple interpretation of the surface temperature/vegetation index space for assessment of surface moisture status. *Rem. Sens. Environ.* 79, 213–224.
- Small, C., 2006. Comparative analysis of urban reflectance and surface temperature. *Rem. Sens. Environ.* 104, 168–189.
- Sobrino, J.A., Jiménez-Muñoz, J.C., Paolini, L., 2004. Land surface temperature retrieval from Landsat TM 5. *Rem. Sens. Environ.* 90 (4), 434–440.
- Stathopoulou, M., Cartalis, C., 2009. Downscaling AVHRR land surface temperatures for improved surface urban heat island intensity estimation. *Rem. Sens. Environ.* 112, 2592–2605.
- Van, D., Griend, A.A., Owe, M., 1993. On the relationship between thermal emissivity and the normalized difference vegetation index for natural surfaces. *Int. J. Remote Sens.* 14, 1119–1131.
- Voogt, J.A., Oke, T.R., 2003. Thermal remote sensing of urban climates. *Rem. Sens. Environ.* 86 (3), 370–384.
- Wan, Z., Dozier, J., 1996. Generalized split-window algorithm for retrieving land-surface temperature from space. *IEEE Trans. Geosci. Remote Sens.* 34, 892–905.
- Wan, Z., Li, Z.L., 1997. A physics-based algorithm for retrieving land-surface emissivity and temperature from EOS/MODIS data. *IEEE Trans. Geosci. Remote Sens.* 35 (4), 980–996.
- Wan, Z., Li, Z.L., 2008. Radiance-based validation of the V5 MODIS land surface temperature product. *Int. J. Remote Sens.* 29 (17/18), 5373–5395, 2008.
- Weng, Q., Fu, P., 2014. Modeling diurnal land temperature cycles over Los Angeles using downscaled GOES imagery. *ISPRS J. Photogrammetry Remote Sens.* 97, 78–88.
- Weng, Q.H., Lu, D.S., Schubring, J., 2004. Estimation of land surface temperature–vegetation abundance relationship for urban heat island studies. *Rem. Sens. Environ.* 89, 467–483.
- Yang, Y., Yao, L., 2009. The influence of urban design factors on urban heat environment in urban residential area with remote sensing. In: Proceedings of the Sixth International Symposium on Multispectral Image Processing and Pattern Recognition, Yichang, China, 30 October–1 November 2009. International Society for Optics and Photonics, Bellingham, WA, USA, p. 74984K, 2009.
- Yang, G.J., Pu, R.L., Zhao, C.J., Huang, W.J., Wang, J.H., 2011. Estimation of subpixel land surface temperature using an endmember index based technique: a case examination on ASTER and MODIS temperature products over a heterogeneous area. *Rem. Sens. Environ.* 115 (5), 1202–1219.
- Yang, G., Pu, R., Huang, W., Wang, J., Zhao, C., 2010. A novel method to estimate subpixel temperature by fusing solar-reflective and thermal-infrared remote-sensing data with an artificial neural network. *IEEE Trans. Geosci. Remote Sens.* 48 (4), 2170–2178.
- Yuan, F., Bauer, M.E., 2007. Comparison of impervious surface area and normalized difference vegetation index as indicators of surface urban heat island effects in Landsat imagery. *Rem. Sens. Environ.* 106, 375–386.
- Zaksek, K., Oštr, K., 2012. Downscaling land surface temperature for urban heat island diurnal cycle analysis. *Rem. Sens. Environ.* 117, 114–124.
- Zhang, Y., 2015. Land Surface Temperature Inversion and Downscaling Research for Landsat 8. Master Thesis. Hohai University, Nanjing, China, 2015.
- Zhan, W., Chen, Y., Zhou, J., Wang, J., Liu, W., Voogt, J., Zhu, X., Quan, J., Li, J., 2013. Disaggregation of remotely sensed land surface temperature: literature survey, taxonomy, issues, and caveats. *Rem. Sens. Environ.* 131, 119–139.
- Zha, Y., Gao, J., Ni, S., 2003. Use of normalized difference built-up index in automatically mapping urban areas from TM imagery. *Int. J. Remote Sens.* 24 (3), 583–594.
- Zhou, D., Xiao, J., Bonafoni, S., Berger, C., Deilami, K., Zhou, Y., Frolking, S., Yao, R., Qiao, Z., Sobrino, J., 2019a. Satellite remote sensing of surface urban heat islands: progress, challenges, and perspectives. *Rem. Sens.* 11 (1), 48.
- Zhou, J., Liu, S., Li, M., Zhan, W., Xu, Z., Xu, T., 2016. Quantification of the scale effect in downscaling remotely sensed land surface temperature. *Rem. Sens.* 8, 975.
- Zhou, P., Han, J., Cheng, G., Zhang, B., 2019b. Learning compact and discriminative stacked autoencoder for hyperspectral image classification. *IEEE Trans. Geosci. Remote Sens.* 1–11.